Available online at www.sciencedirect.com
SCIENCE DIRECT®
Inorganica Chimica Acta 359 (2006) 4043–4052
Inorganica Chimica Acta
www.elsevier.com/locate/ica

Luminescent $CeCl_3$ nanoparticles by Tris(1,1,1,5,5,5-hexafluoro-2,4-pentanedionato)cerium diglyme photolysis in chlorinated solvents

Salvatore Giuffrida [a,*], Guglielmo G. Condorelli [a], Lucia L. Costanzo [a], Giorgio Ventimiglia [a,b], Maria Favazza [a], Salvatore Petralia [a,b], Ignazio L. Fragalà [a]

[a] *Dipartimento di Scienze Chimiche, Università degli Studi di Catania and INSTM UdR di Catania, V.le A. Doria 6, 95025 Catania, CT, Italy*
[b] *LoC R&D, Microfluidic Division-CPG ST Microelectronics, I-95121, Catania, Italy*

Received 9 March 2006; received in revised form 2 May 2006; accepted 13 May 2006
Available online 2 June 2006

Abstract

Irradiation of [Ce(hfac)$_3$(diglyme)] (hfac = 1,1,1,5,5,5-hexafluoro-2,4-pentanedionato and diglyme (DG) = 2,5,8,11,14-pentaoxapentadecane) in chlorinated solvents (CH_2Cl_2, CCl_4) with UV light led to luminescent colloidal $CeCl_3$ that was characterized by transmission electron microscopy (TEM) analysis. When a substrate, quartz or silicon was present in the reaction cell, photoluminescent films were obtained, containing either pure $CeCl_3$ or mixtures of $CeCl_3$, CeF_3 and CeOx in function of the experimental parameters of irradiation. Nanostructured and luminescent pure $CeCl_3$ films were obtained by irradiation of the cerium complex in CCl_4 at high intensity light for a few minutes. The films were characterized by X-ray diffraction (XRD), Energy dispersive X-ray (EDX), X-ray photoelectron spectroscopy (XPS), TEM, scanning electron microscopy (SEM) and atomic force microscopy (AFM). The kinetics of the [Ce(hfac)$_3$(diglyme)] solution photodegradation, followed by UV spectrophotometry and spectrofluorimetry, pointed to $CeCl_3$ formation by a solvent-initiated reaction, whereas the other inorganic compounds were the products of side reactions.

Keywords: Photochemistry; Luminescence; Nanoparticles; Deposition; Cerium chloride

1. Introduction

In the last decade, a great interest has been shown in trivalent lanthanide rare-earth ions, such as cerium(III), because of their luminescence properties. These ions are involved in the fabrication of electroluminescent [1] and photoluminescent [2,3] devices. They could be used in projecting new solid-state lasers in the ultraviolet and blue spectral domains. The emission from such types of ions is strictly connected with the host crystal. Thus, rare earth activated luminescent materials have been studied in their crystalline and powder form for use in cathodic ray tube (CRT) phosphors and other related applications.

In general, these luminescent ions are used as dopants for second group metal halide host matrices. Studies on Ce^{3+} luminescence properties in alkaline earth (Ca, Sr, Ba) chlorides [4] showed that the energy shift of the emission depends on the structure of the host lattice. Moreover, it has been proven that the particles at the nanometer level have an improved quality with respect to their potential application to various optical, electrical, mechanical and catalytic activities [5]. It is known that the dimensions of phosphor particles are crucial in the enhancement of the luminescence [6,7]. Many techniques have been used to prepare thin films of cerium-containing materials, such as evaporation methods, sputtering, spray pyrolysis technique [8], whereas only a CVD technique has been reported to obtain pure cerium fluoride films [9]. To the best of our knowledge, nowadays no method has been reported in

* Corresponding author. Tel.: +39 0957385063; fax: +39 095580138.
E-mail address: sgiuffrida@unict.it (S. Giuffrida).

0020-1693/$ - see front matter © 2006 Elsevier B.V. All rights reserved.
doi:10.1016/j.ica.2006.05.022

the literature to obtain pure films of $CeCl_3$. In this paper, we report about the fabrication of colloidal particles and nanostructured films of pure $CeCl_3$ by using a simple and inexpensive method of photochemical deposition from liquid phase [10,11].

2. Experimental

[Ce(hfac)$_3$(diglyme)] was synthesized according to the literature [12]. CH_2Cl_2 and CCl_4 were of analytical grade with H_2O of about 0.02% or 0.01%, respectively. *Warning:* CCl_4 is toxic for inhalation and dangerous for ozone layer.

$CeCl_3$ commercial anhydrous powder was purchased from Aldrich.

Irradiation was performed with cuvettes of optical path of 1 cm, whereas the measurements were carried out with cuvettes of optical path 0.1, 0.5 or 1 cm, depending on the concentration of the solution.

For light source, a Rayonet photochemical reactor, equipped with a variable number of lamps (Italquartz) with monochromatic emission at either 254 nm or at 300 nm, was used. The light intensity, measured by a ferric oxalate actinometer [13], was in the range of 1.08–27 mW cm^{-2} (4.0×10^{-7}–1.0×10^{-5} Nhν min^{-1}) for 254 nm and 6 mW cm^{-2} (2.6×10^{-6} Nhν min^{-1}) for 300 nm. When necessary, a screen with a suitable window was used.

The quantum yields were calculated by ratio between initial disappearance rate of the complex and number of absorbed photons by reactive species.

UV–Vis absorption spectra were measured using a double beam Jasco-V560 spectrophotometer.

For the luminescence spectra, a SPEX Fluorolog 111 instrument, equipped with a solid sample holder, was used. The luminescence spectra are recorded within the linear range of the photo multiplier response.

Films were obtained on quartz and Si(1 0 0) substrates of dimensions 0.5×2 cm, using solutions of concentration 10^{-3} mol L^{-1} in CCl_4. To obtain substrates with just one side covered, the quartz plate was deposited on the bottom of an horizontally disposed cuvette and irradiated from below with a single lamp; whereas to cover both sides, the substrate (silicon or quartz) was put along the diagonal of the cuvette and irradiated into the photochemical reactor (Fig. 1).

After photochemical film deposition, the substrates were washed with pure solvent to remove possible organic substances, such as free ligand or decomposition organic products, adsorbed on the surface.

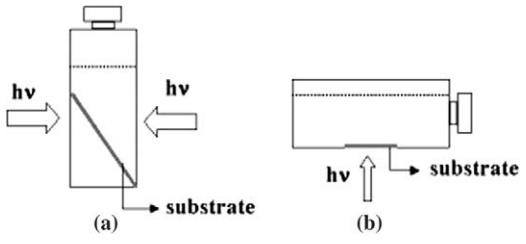

Fig. 1. Cuvettes for $CeCl_3$ film deposition: (a) on both sides of quartz or silicon substrates; (b) on just one side of quartz substrate.

Some $CeCl_3$ deposition, depending upon the starting complex concentration, occurred on the interior walls of the cuvette. However, this did not prevent the light from attaining the solution bulk.

For the chemical characterization of the colloidal particles, a deposit was obtained upon solvent evaporation, on suitable substrate, of some drops of the colloidal solution.

XPS measurements were performed with a PHI 5600 Multy Technique System equipped with an Al standard X-ray source operating at 14 kV and a hemispherical analyzer. The electron take off angle was 45°. Binding energy (BE) data were calibrated on C 1s at 285 eV.

XRD measurements were made with a Bruker AXS D5005 X-ray diffractometer.

Chemical composition of film and powders was evaluated by EDX analysis using a windowless IXRF solid state detector and the surface morphology was examined through scanning electron microscopy (SEM) using a LEO SUPRA 55VP equipped with a field emission gun.

AFM images were acquired with a microscope SOLVER-Pro by Nt-MDT.

TEM images of cerium chloride nanoparticles were obtained by means of a FEG JEM 2010F instrument with a field emission gun operating at 200 kV. The electro-optical configuration guarantees ultra high spatial resolution (0.19 nm). This microscope is equipped with the GIF (Gatan Image Filter) apparatus, which allows realizing images filtered to narrow windows of the electron energy loss spectrum.

3. Results and discussion

3.1. Photolysis of [Ce(hfac)$_3$(diglyme)] in chlorinated solvents

Preliminary experiments regarding the photochemical reactivity of [Ce(hfac)$_3$(diglyme)] at UV light showed that in the non-chlorinated solvents, such as methanol and acetonitrile, the complex can be considered photochemically inert, because it underwent slow degradation with quantum yield $<10^{-4}$. In the chlorinated solvents, like CH_2Cl_2 and CCl_4, photolysis occurred, leading mainly to colloidal cerium chloride. When a substrate was present in the reaction cell, luminescent films containing $CeCl_3$ were obtained.

The photoreaction kinetics were followed by spectrophotometric and fluorimetric analysis. In both solvents, the electronic spectrum of [Ce(hfac)$_3$(diglyme)] exhibits a band due to the intra-ligands π_L to π_L^* transitions (IL) ($\lambda_{max}=306$ nm and 308 nm, molar absorptivity (ε) = 28 000 L mol^{-1} cm^{-1} and 30 000 L mol^{-1} cm^{-1} in CH_2Cl_2 and in CCl_4, respectively), as found in other complexes with betadiketonate ligands [14,15]. A shoulder, due to cerium(III) ion electronic transitions (5d–4f), is present at about 280 nm. The absorption of the free ligand in the

protonated form is centred at 274 nm ($\varepsilon = 6700$ L mol^{-1} cm^{-1}) in both solvents.

The irradiation of [Ce(hfac)$_3$(diglyme)] solutions provoked spectral changes showing the bleaching of the absorbance maximum and the growth of a band at 274 nm, this latter being typical of the protonated ligand Hhfac (Fig. 2). The isosbetic point at about 290 nm proved that the process was occurring with constant stoichiometry without side reactions. With the naked eye the irradiated solutions appeared clear, but a diffuse absorbance above 350 nm, that was better observed as the complex concentration increased, indicated the presence of colloidal particles and the formation of a slight deposit on the inner walls of the cuvette.

As the absorbance maximum decreased, the characteristic emission of the $CeCl_3$ [16,17] appeared and increased with reaction time (Fig. 3). This emission exhibited high maxima at 355 nm and at 370 nm, which were shifted about 12 nm towards the visible region with respect to the luminescence, recorded with commercial $CeCl_3$ powder, dispersed in CCl_4.

These findings allowed us to deduce that the following photochemical reaction occurred:

$$[Ce(hfac)_3(diglyme)] \xrightarrow[CH_2Cl_2,CCl_4]{\text{UV light}} CeCl_3 + 3Hhfac + diglyme$$

Because Hhfac and diglyme are quite soluble in chlorinated solvents, the colloidal particles were constituted of the $CeCl_3$ as confirmed by XPS results which are discussed later in this paper.

For 254 nm irradiation of solutions of concentrations less than 3×10^{-4} mol L^{-1}, at all times of irradiation the free ligand concentration was three times more than the disappeared complex concentration ($-\Delta$[complex] = 1/3 Δ[ligand]). The isosbestic point remained constant, until the complete release of the ligands; thus the substitution hfac$^-$ with Cl$^-$ occurred without any side reaction. The films obtained in these conditions were constituted only by $CeCl_3$ (see below).

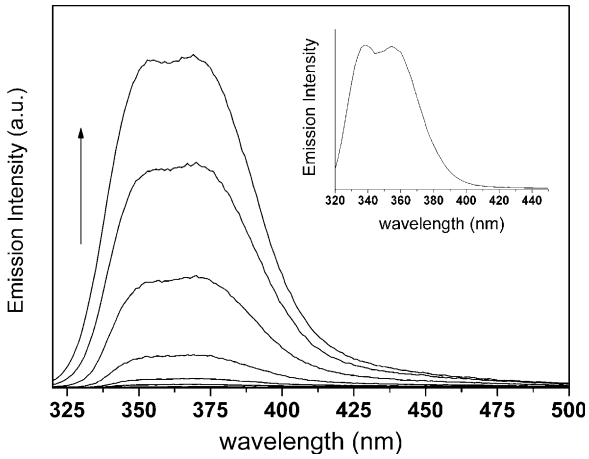

Fig. 3. Emission spectra ($\lambda_{exc} = 300$ nm) of $CeCl_3$ colloidal particles in CCl_4, formed at 254 nm, at various irradiation times ($t_{irr} = 45$ s). In the inset: commercial $CeCl_3$ powder dissolved in CCl_4.

Prolonged irradiation provoked slow decomposition of the released ligand, detectable by a decrease of the absorbance at 274 nm and a shift of the isosbestic point.

When solutions of concentration higher than 3×10^{-4} mol L^{-1} were irradiated, decomposition of the released ligands occurred before the complete photolysis of the complex. The films obtained in these conditions contained chloride, fluoride and oxide of cerium (see below).

The kinetics of the photodegradation at 254 nm were investigated in function of the initial complex concentration and incident light intensity. The results showed that the absorbance maximum of the complex (thus its concentration) decreased linearly with irradiation time (Fig. 4) for most of the reaction. This indicated kinetics of zero order and a constant rate of reaction, evaluated as $-$d[complex]/dt. Besides this, by increasing the solution concentration, the plot slopes (thus the reaction rate) decreased in CH_2Cl_2, whereas it remained constant in CCl_4. For the solutions reported in Fig. 4a, the rate values are 7.2×10^{-6}, 4×10^{-6} and 1.5×10^{-6} mol L^{-1} min^{-1} from bottom to top; for the

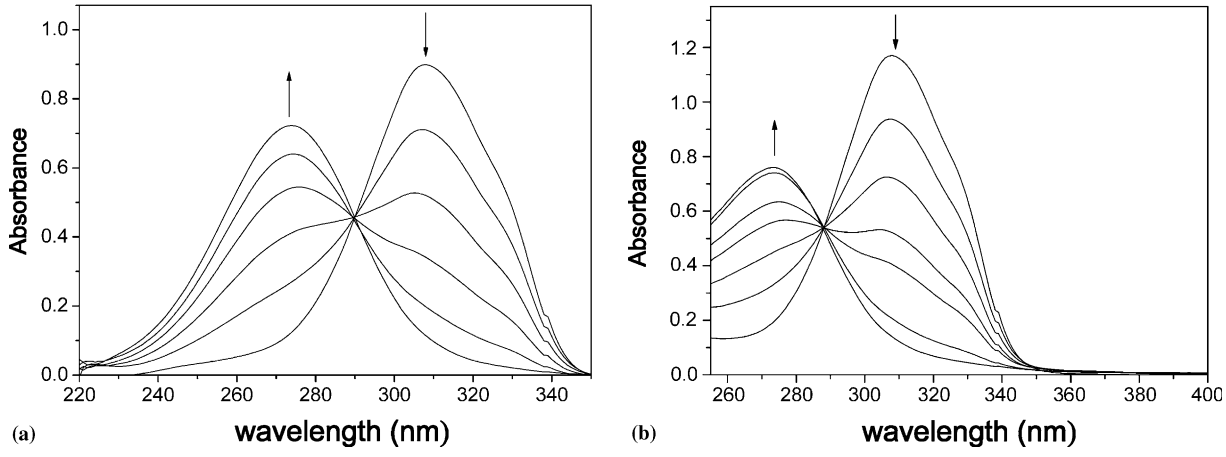

Fig. 2. Spectral changes of [Ce(hfac)$_3$(diglyme)] (3.5×10^{-5} M) at various irradiation times. $\lambda_{exc} = 254$ nm. $I = 5.4$ mW cm^{-2}: (a) CH_2Cl_2 ($t_{irr} = 3$ min); (b) CCl_4 ($t_{irr} = 45$ s).

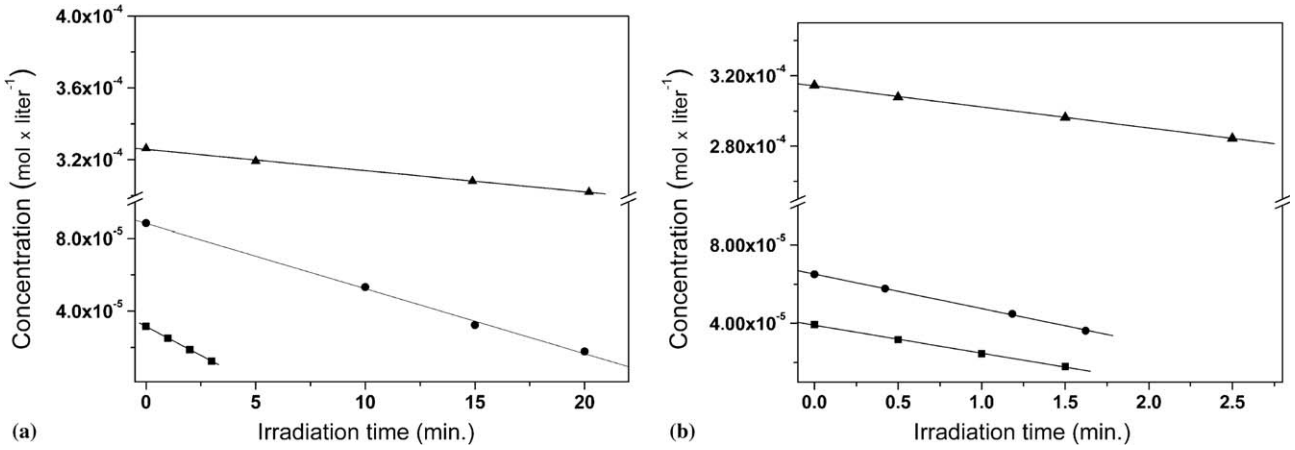

Fig. 4. Change of the complex concentration vs. the irradiation time. $\lambda_{exc} = 254$ nm. (a) CH_2Cl_2, $I = 5.4$ mW cm^{-2}; (b) CCl_4, $I = 1.08$ mW cm^{-2}.

solutions reported in Fig. 4b, the rate value is 1.5×10^{-5} mol L^{-1} min^{-1} in all cases.

At constant concentration, the rate reaction increased linearly with the light intensity in the range 4×10^{-7}–2×10^{-6} N$h\nu$ min^{-1} (1.08–5.4 mW cm^{-2}) in both solvents (Fig. 5).

The photochemical behaviour of the cerium complex is typical of a solvent-initiated reaction, whose rate depends on the fraction of light absorbed by the solvent; thus it decreases with the complex concentration. The literature contains examples of such types of solvent-initiated reactions for chlorinated solvents [18], in which the solvent absorbs the UV light to give homolytic cleavage of C–Cl bond with production of chlorinated radicals leading to HCl and subsequent ligand substitution.

In the present case, this assertion was confirmed by suitable experiments showing that the preirradiated solvent was able to provoke ligand substitution with chloride ion in the complex, which was added subsequently.

In dichloromethane, only 2.5% of the 254 nm light is absorbed by the solvent. Nevertheless, a solvent-initiated

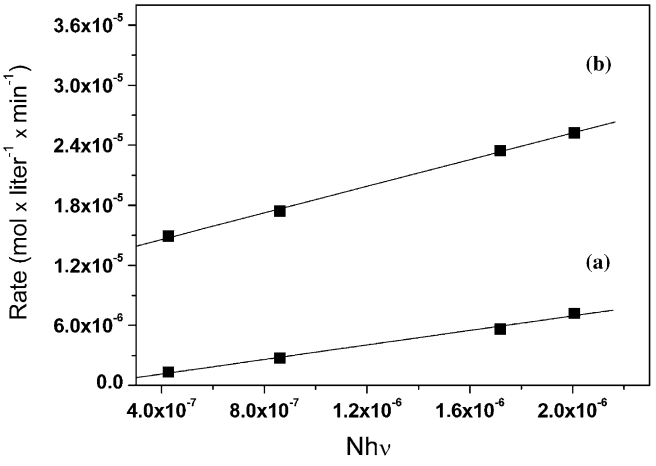

Fig. 5. Reaction rate as a function of incident light intensity. [complex] $= 3 \times 10^{-5}$ mol L^{-1}, $\lambda_{exc} = 254$ nm. (a) CH_2Cl_2; (b) CCl_4.

$$CH_2Cl_2 \xrightarrow{h\nu} CH_2Cl\bullet + Cl\bullet \quad (1)$$

$$CH_2Cl_2 + Cl\bullet \longrightarrow HCl + CHCl_2\bullet \quad (2)$$

$$CH_2Cl\bullet + CH_2Cl_2 \longrightarrow CH_3Cl + CHCl_2\bullet \quad (3)$$

Scheme 1.

reaction can occur both because it is a chain reaction that requires very little light input and because the wavelength distribution of the light source can provide some flux of light below 254 nm. The observed decrease of the reaction rate with concentration of complex is due to the increase of the 254 nm absorbance of the latter, with consequent decrease of the light fraction absorbed by the solvent. The CH_2Cl_2 provides HCl, which undergoes Cl^-–$hfac^-$ substitution, according to Scheme 1, proposed previously [19].

In the presence of oxygen the $CHCl_2^{\cdot}$ radical undergoes decomposition leading, through a complex mechanism, to the following reaction:

$$CHCl_2^{\cdot} \xrightarrow{O_2} CO + HCl + \text{other products} \quad (4)$$

Further confirmation of the proposed mechanism was provided by some experiments showing the role of oxygen in the process. It was found that by lessening the dissolved oxygen in solution by means of nitrogen bubbling, the complex degradation rate decreased with the time of deaeration.

The linearity of the dependence of the rate reaction on the light intensity is in accordance with a mechanism involving radical termination steps, which do not affect the rate [20].

The quantum yield of $CeCl_3$ formation, calculated by values of the rate and of light fraction absorbed only by dichloromethane, is $\Phi_{CH_2Cl_2} = 0.47$.

As regarding the CCl_4, earlier investigations [21,22] have evidenced that the direct and sensitised photolysis of CCl_4 leads to $Cl^{\cdot}$ and $CCl_3^{\cdot}$ radicals. The radical $CCl_3^{\cdot}$ leads to

HCl through several microreactions, including the formation of $CCl_3O_2^{\bullet}$ and $COCl_2$ intermediates.

In the presence of H_2O traces, the phosgene undergoes hydrolysis to HCl (Scheme 2).

The proposed mechanism has been confirmed by further experiments carried out in deaerated CCl_4 solution (by vacuum-nitrogen line). In these conditions, the degradation complex was completely stopped suggesting that the $CCl_3^{\bullet}$ and $Cl^{\bullet}$ radicals are inactive chlorinating agents in this case.

Since the radiation of 254 nm can be considered totally absorbed by CCl_4, the rate reaction is independent of complex concentration. The quantum yield, calculated by the reaction rate and the light intensity, is $\Phi_{CCl_4} = 0.11$.

For irradiation at 300 nm, a wavelength not absorbed by dichloromethane, substitution $hfac^{-}$–Cl^{-}, can occur through a different pathway, involving a complex initiated and solvent assisted reaction. This pathway involves the interaction between the excited IL states of the complex and the chlorinated solvent. The excited state of the ligand could transfer an electron [23,24] to the chlorinated solvent, which manifests the capability to accept an electron [25,26], according to Scheme 3.

The electron transfer leads to chloride anion that can bond with the positive fragment of cerium and produce $CeCl(hfac)_2$. The radical $hfac^{\bullet}$ abstracts hydrogen from the solvent, giving the ligand Hhfac and the radical $CHCl_2^{\bullet}$. Both $CHCl_2^{\bullet}$ and $CH_2Cl^{\bullet}$ (Scheme 3) lead to HCl according to Scheme 1. The quantum yield at 300 nm, based on the light absorbed only by complex, is very small. Its value is 2×10^{-4}.

As regarding the CCl_4, $CeCl_3$ formation occurred with preirradiated solvent both at 254 and 300 nm; thus the process was solvent initiated at both wavelengths. The monochromatic radiation of 300 nm is not absorbed by the CCl_4, but the commercial lamps contain little percentage of radiations of shorter wavelengths which are responsible for the photoreaction.

For a useful comparison, the rate values of complex degradation are reported in Table 1.

3.2. Chemical and morphological characterization of deposited films and colloidal nanoparticles

Films on quartz and silicon substrates and colloidal particles have been obtained by irradiating either CH_2Cl_2 or CCl_4 solutions of the [Ce(hfac)$_3$(diglyme)] at 254 nm, at which wavelength the photodegradation rate of the complex was much higher than at 300 nm (Table 1).

XRD analysis of colloidal particles and films obtained after a short irradiation time, just to allow the release of ligands without their decomposition (see above), indicated that the deposit is either amorphous or with grain sizes too small to give significant diffraction peaks. Thus, no useful information about composition of the deposit was given by X-ray diffraction investigation.

The nature of the deposit was, therefore, investigated by XPS analysis. High resolution XPS spectra in the relevant regions of binding energy (BE) are shown in Fig. 6 for both films and colloidal particles. In both cases, the Ce 3d feature (Fig. 6a) shows a complex structure consisting of a main Ce $3d_{5/2}$–Ce $3d_{3/2}$ spin–orbit doublet (around 886.6 eV and 905.4 eV, respectively). These BEs are consistent with the presence of Ce^{3+} ion of $CeCl_3$ [27] compound. Note that each Ce 3d spin–orbit component consists of two features due to a ground state (GS) $3d_{5/2}$–$3d_{3/2}$ photoemission and a lower BE shoulder due to a charge transfer (CT) photoemission [27,28].

The BE values of the Cl $2p_{3/2-1/2}$ spin–orbit doublet (198.7 eV and 200.4 eV) are consistent with the presence of $CeCl_3$. A slight contamination of organic fluorine (BE = 689 eV) was also observed, but no significant inorganic fluorides (at about 685 eV) were detected. The O 1s region shows a band at 532.5 eV associated with oxygen bonded to Si in SiO_2 of the substrate [29].

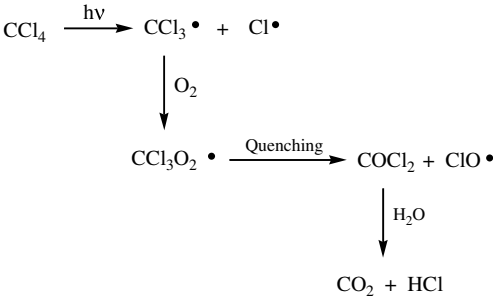

Scheme 2.

Table 1
Rate values (mol L^{-1} min^{-1}) of [Ce(hfac)$_3$(diglyme)] photodegradation

Solvent	λ_{254} (nm)	λ_{300} (nm)
CH_2Cl_2	7.2×10^{-6}	1.3×10^{-7}
CCl_4	2.5×10^{-5}	1×10^{-6}

[complex] = 3×10^{-5} mol L^{-1}; $I_{254} = 5.4$ mW cm^{-2}; $I_{300} = 5.75$ mW cm^{-2}.

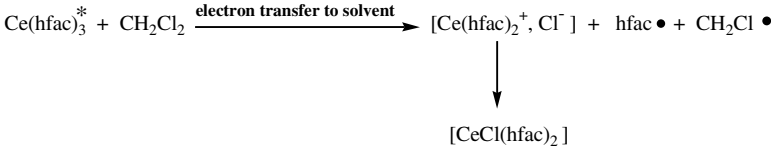

Scheme 3.

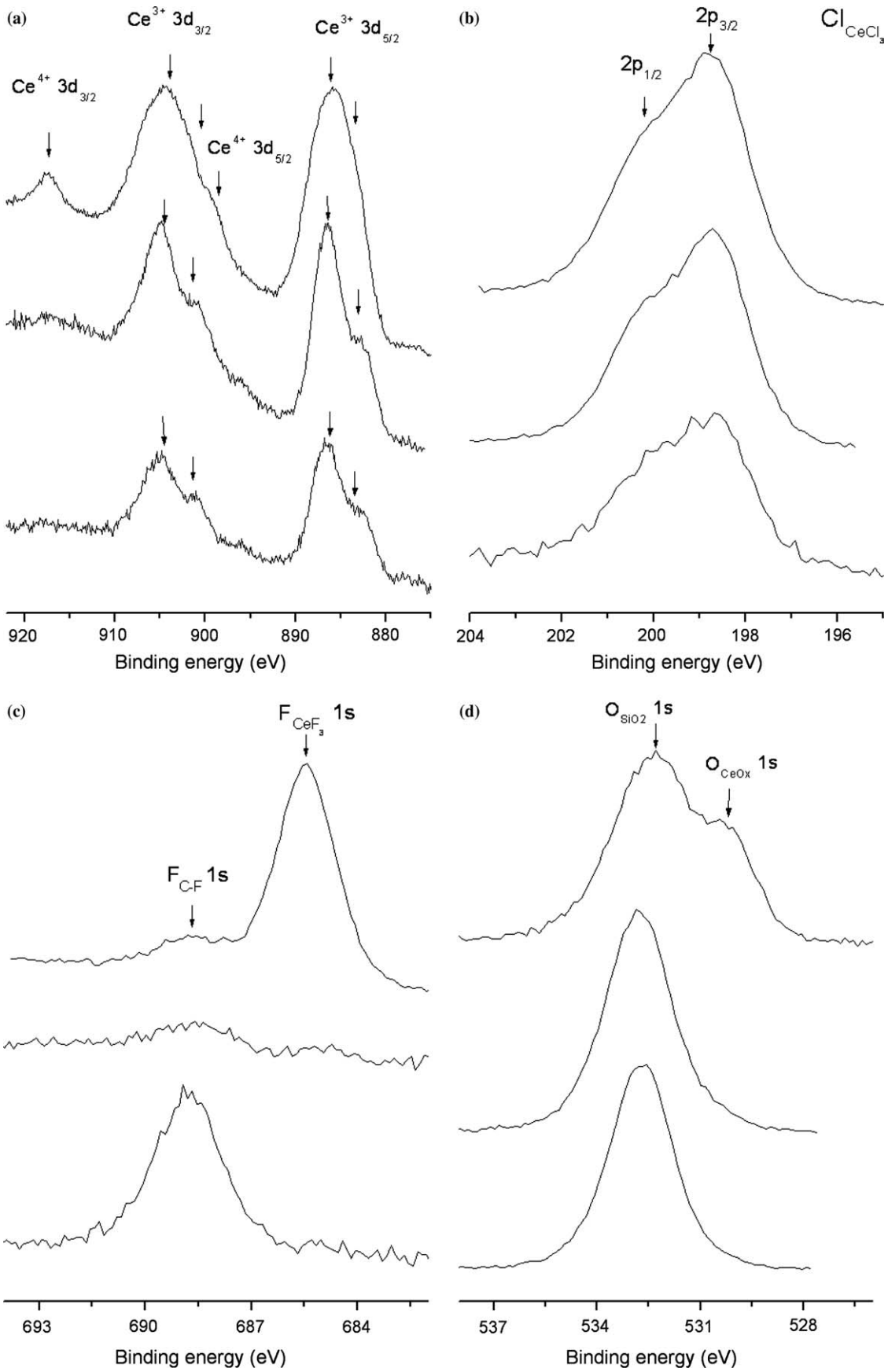

Fig. 6. High resolution photoemission (a) Ce 3d, (b) Cl 2p, (c) F 1s and (d) O 1s. Spectral regions (from bottom to top) of colloidal particles; films from irradiated solutions, before ligand decomposition; films from irradiated solution, after ligand decomposition.

The films obtained by deposition from solutions, after photodecomposition of the released ligands, consisted of various compounds. The photoemission Ce 3d spectral region (Fig. 6a, top) consisted of the main Ce $3d_{5/2}$–Ce $3d_{3/2}$ spin–orbit doublet typical of the Ce^{3+} ion, even though the broadened shape is consistent with the presence of more than one compound. In addition, a lower intensity Ce $3d_{5/2}$–Ce $3d_{3/2}$ spin–orbit doublet (at 899 eV and 917 eV, respectively) is indicative of the presence of Ce^{4+} ion (i.e. CeO_2) [28]. The BE values of the Cl $2p_{3/2-1/2}$ spin–orbit doublet (198.7 eV and 200.4 eV) and of the F 1s (685.4 eV), typical of inorganic chloride and fluoride compounds, indicated the presence of both $CeCl_3$ and CeF_3. The O 1s XPS region consists of two components: O_{SiO_2} at 532.5 eV associated with oxygen bonded to Si in SiO_2 of the substrate [30] and O_{CeO_2} at 530.0 eV associated with the oxygen bonded to cerium in CeO_2 [30].

It is worth noting that the CeF_3 and CeOx compounds, present in these films, are not formed by direct photochemical reaction, starting from the excited complex states, but are formed indirectly. The fluoride can be formed by an attack of fluorinated fragments of the decomposed ligand on the starting complex or its intermediates. The oxide can derive from an attack of peroxy-radicals on the starting complex or its derivates.

The surface Cl/Ce atomic ratios of various samples have been determined from the intensity of XPS bands using Wagner sensitivity factor [31] corrected for the instrument transmission function. The Cl/Ce ratio of colloidal particles and films obtained for short irradiation time is about 3 ± 0.5 as expected for $CeCl_3$. In the case of sample obtained for long irradiation and, therefore, after ligand decomposition, the Cl/Ce ratio decreases until 1.5 due to the presence of other Ce-containing compounds (CeF_3 and CeOx).

Finally, note that for all films, XPS analysis showed the Si 2p signal of the substrate, thus indicating that substrate surface is not fully covered and suggesting the presence of $CeCl_3$ islands.

The chemical nature of the bulk of deposit was determined by EDX analysis. According to surface XPS analysis, the bulk of films and colloidal nanoparticles obtained for short irradiation is made of cerium and chlorine with a Cl/Ce atomic ratio close to 3 ± 0.1, whilst the Cl/Ce ratio decreases down to 1 for samples obtained for long irradiation.

The surface morphology of films deposited on silicon and quartz substrates has been examined with SEM analysis. Fig. 7 shows SEM micrographs of films obtained under various experimental conditions.

EDX analysis performed in points 1 indicates that the islands are constituted by $CeCl_3$, whilst no significant Ce and Cl amounts have been detected for points 2.

In all cases, it results in particle aggregation with formation of islands, as already suggested by XPS results (see above). Pointing to the islands, the performed EDX analysis confirmed that they are made of $CeCl_3$, whilst out of the $CeCl_3$ islands the amounts of the Ce and Cl are negligible.

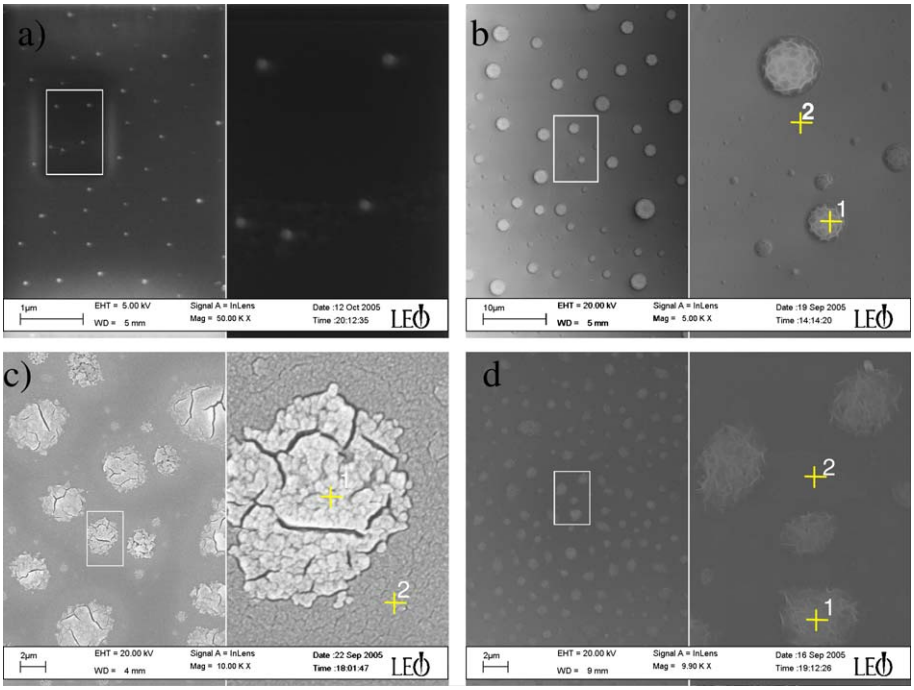

Fig. 7. SEM micrographs of various films: (a) deposited on Si at high light intensity ($I = 27$ mW cm^{-2}, $t_{irr} = 45$ s) from solutions 10^{-4} mol L^{-1}; (b) deposited on Si at high light intensity ($I = 27$ mW cm^{-2}, $t_{irr} = 3$ min) from concentrated solution 10^{-3} mol L^{-1}; (c) deposited on quartz at low light intensity ($I = 6$ mW cm^{-2}, $t_{irr} = 6$ h) from concentrated solution 10^{-3} mol L^{-1} and covered with Au layer for the SEM analysis; (d) deposited on Si after ligand decomposition ($I = 6$ mW cm^{-2}, $t_{irr} = 12$ h) from concentrated solution 10^{-3} mol L^{-1}.

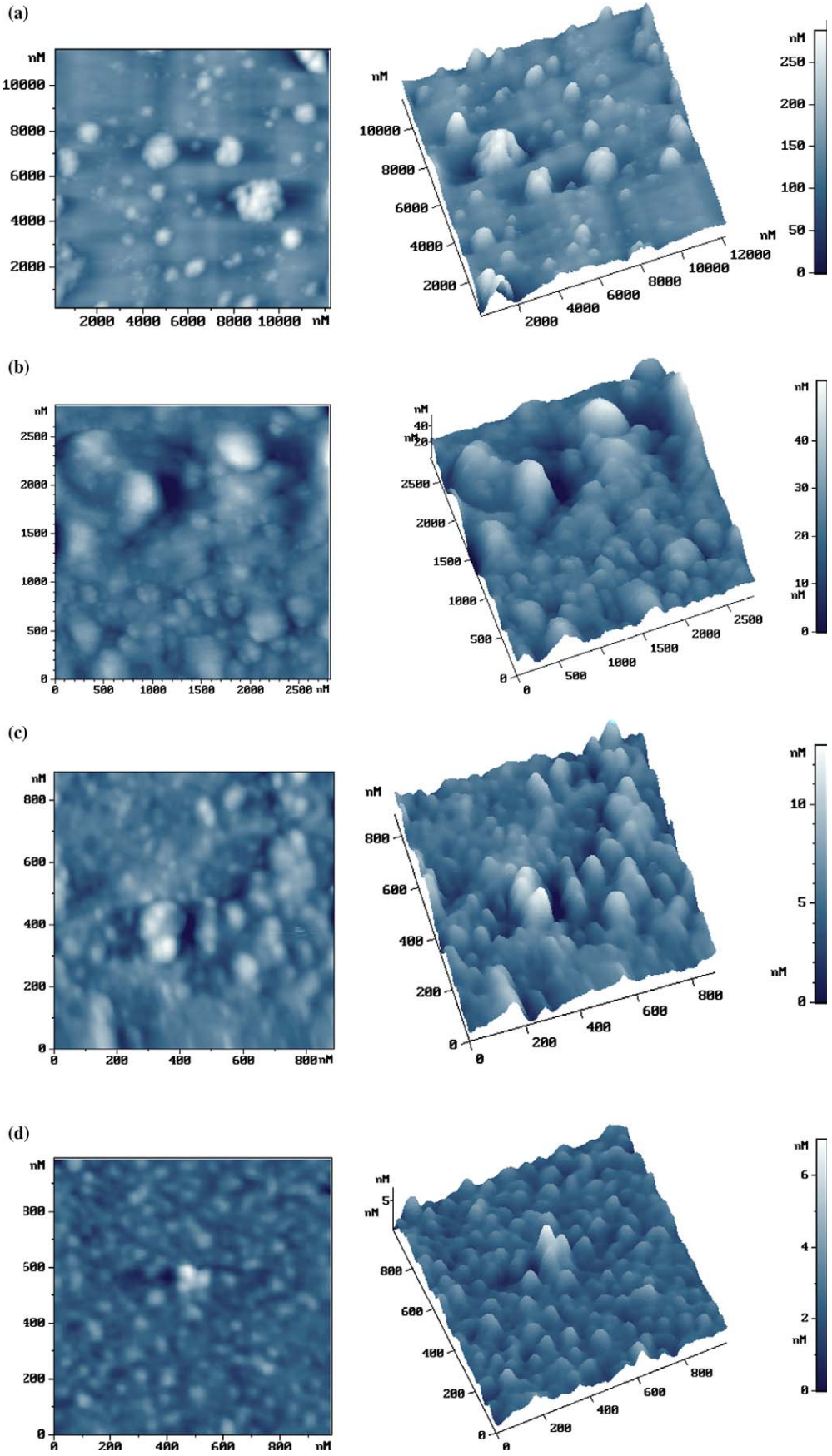

Fig. 8. AFM images of pure $CeCl_3$ films deposited from solutions 10^{-3} mol L^{-1} (a) and 10^{-4} mol L^{-1} (b–d) irradiated with light of various intensities: (a) $I = 6$ mW cm^{-2}, $t_{irr} = 6$ h; (b) $I = 1.08$ mW cm^{-2}, $t_{irr} = 8$ min; (c) $I = 5.4$ mW cm^{-2}, $t_{irr} = 3$ min; (d) $I = 27$ mW cm^{-2}, $t_{irr} = 45$ s.

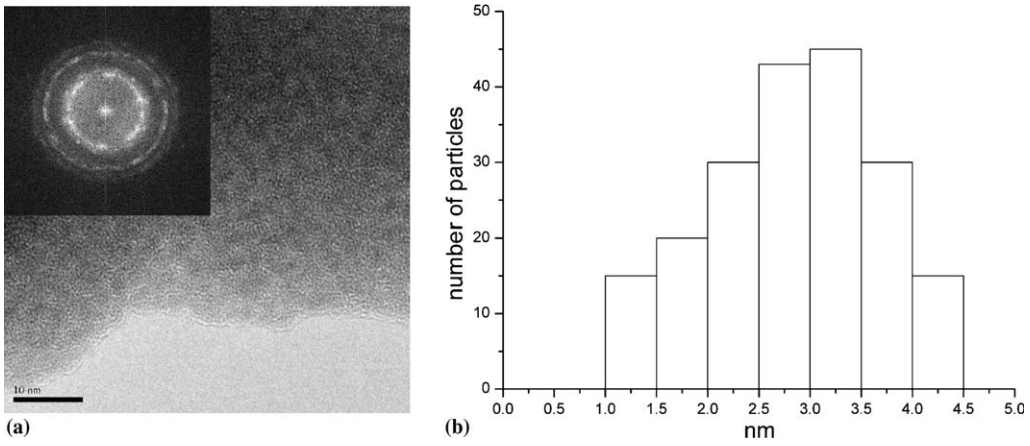

Fig. 9. (a) TEM analysis on a sample of colloidal $CeCl_3$. (b) Particle size distribution.

For high light intensity ($I = 27$ mW cm^{-2}), but short deposition times and low solution concentrations ($t_{irr} = 1$ min and 10^{-4} mol L^{-1}), the films show the presence of monodispersed particles with a size of about 20 nm.

For higher concentration (10^{-3} mol L^{-1}), the particles aggregate to form islands with sizes of some microns.

The roughness of the pure $CeCl_3$ films obtained on quartz has been determined by AFM measurements. The results showed that smoother films can be obtained by increasing the $CeCl_3$ formation rate that can be obtained at low solution concentration with increasing light intensity (Fig. 8).

The films obtained from solutions 10^{-3} mol L^{-1} (Fig. 8a) show the presence of islands with an average height (R_{mead}) of 0.2 μm. Fig. 8b–d shows three examples of the AFM images of $CeCl_3$ films deposited from CCl_4 solutions 10^{-4} mol L^{-1} and irradiated with increasing light intensity. The films obtained by irradiation with a light of lowest intensity show a rough surface (Fig. 8b) with an average peak-to-peak distance (R_{mead}) of about 24 nm and a roughness of 6.7 nm. Films obtained using light of middle intensity show less rough surfaces (Fig. 8c). The R_{mead} value is 5.4 nm with a roughness of 1.6 nm. The third sample, obtained from solution irradiated with the highest light intensity, shows a surface much flat and homogeneous (Fig. 8d). The R_{mead} is 2.4 nm with a roughness of 0.6 nm. Both values are significantly lower than those observed for samples deposited by adopting less intense irradiation. It is important to evidence that the third sample is constituted of much smaller (40 ± 10 nm) and more homogeneous particles, compared to those of the other two samples. This finding supports the idea that, in general, the right tuning of the irradiation conditions leads to the formation of nanostructured films.

TEM analysis was performed on the colloidal particles obtained by irradiating complex solution 10^{-3} mol L^{-1} in CCl_4 for 4 min. Samples have been dried on copper grids. Fig. 9a shows TEM micrographs of the $CeCl_3$ nanoparticles forming clustered aggregates. However, note that it is not clear how much coagulation occurs in the initial solutions and how much occurs during solvent evaporation when the TEM grids are prepared. TEM image shows the presence of nanoclusters characterized by a size distribution (Fig. 9b) with an average diameter of 2.9 nm and a dispersion σ of 1.0 nm. The inset is the forward of the Fourier transformation (FFT) of the high resolution TEM image which shows that this sample is a fcc structure with diffraction rings at 3.17 Å and 2.70 Å due to the (1 1 1) and (2 0 0) planes, with a reticular parameter of $a = 5.43$ Å.

4. Conclusion

The above results evidence the close connection between morphology, composition and grain size of nanoparticles and films with the experimental conditions used to obtain deposition. Luminescent films and particles of pure $CeCl_3$ were produced by carrying out the photochemical reaction in controlled conditions of initial concentration, of solvent nature, of light intensity, of irradiation time, in order to avoid photodecomposition of the released ligands, that would bring to other inorganic compounds of cerium. By right tuning of the cited experimental parameters, nanostructured films of pure $CeCl_3$ were obtained from CCl_4 solutions, when the films were formed in very short irradiation time; thus when the $CeCl_3$ formation rate was very high.

In conclusion, this paper shows that the photochemical method was very suitable to obtain films with the desired characteristics, by exploiting an inexpensive and simple technique which works at room temperature. This last characteristic can be very important, since it allows to use several types of substrates, as functionalised substrates. It is noteworthy to emphasize that the study of the reaction mechanism in solution is the basis supporting all research in the field of photodeposition from liquid phase, since the knowledge of the photo reaction mechanism is the only way to select the most suitable conditions to improve the film qualities.

Acknowledgment

The authors thank the MIUR (FIRB 2003 research program) for financial support.

References

[1] T.A. Oberacker, H.W. Schock, J. Cryst. Growth 159 (1996) 935.
[2] K.R. Reddy, K. Annapurna, S. Buddhudu, Mater. Lett. 28 (1996) 489.
[3] W. Jia, Y. Yang, F. Fernandez, X. Wang, S. Huang, W.M. Yen, Mater. Sci. Eng. C16 (2001) 55.
[4] W.M. Li, M. Lesela, Chem. Phys. Lett. 311 (1999) 167.
[5] C.J. Brinker, G.W. Scherer, in: Sol–gel Science: The Physics and Chemistry of Sol Gel Processing, Academic Press, New York, 1990.
[6] W.M. Li, M. Lesela, Mater. Lett. 28 (1996) 491.
[7] P.K. Sharma, M.H. Jilavi, R. Nass, H. Shumidt, J. Lumin. 82 (1999) 187.
[8] A. Esparza, M. Garcia, C. Falcony, Thin Solid Films 325 (1998) 14.
[9] R. Lo Nigro, G. Malandrino, I.L. Fragalà, M. Bettinelli, A. Spedini, J. Mater. Chem. 12 (2002) 2816.
[10] A. Peled, Laser Eng. 6 (1997) 41.
[11] S. Giuffrida, G.G. Condorelli, L.L. Costanzo, I.L. Fragalà, G. Ventimiglia, G. Vecchio, Chem. Mater. 16 (7) (2004) 1260.
[12] G. Malandrino, F. Castelli, I. Fragalà, Inorg. Chim. Acta 224 (1994) 203.
[13] J. Calvert, J.N. Pitts, in: Experimental Methods in Photochemistry, Wiley, New York, 1966, p. 783.
[14] B. Marciniak, G.E. Buono-Core, J. Photochem. Photobiol. A: Chem. 52 (1990) 1.
[15] H. Nakanishi, H. Morita, S. Nagakura, Bull. Chem. Soc. Jpn. 51 (6) (1978) 1723.
[16] B. Keller, J. Legendziewicz, J. Glinski, S. Samela, J. Alloys Compd. 300-301 (2000) 334.
[17] A.S. Voloshinovskii, P.A. Rodnyi, O.T. Antonyak, N.S. L'vov, Fiz. Tverdogo Tela 36 (1994) 436.
[18] P.E. Hoggard, Coord. Chem. Rev. 159 (1997) 235.
[19] S. Giuffrida, L.L. Costanzo, G.G. Condorelli, G. Ventimiglia, I.L. Fragalà, Inorg. Chim. Acta 358 (2005) 1873.
[20] S. Whang, T. Estrada, P.E. Hoggard, Photochem. Photobiol. 79 (4) (2004) 356.
[21] P.E. Hoggard, A. Vogler, Inorg. Chim. Acta 348 (2003) 229.
[22] P.E. Hoggard, M. Gruber, A. Vogler, Inorg. Chim. Acta 346 (2003) 137.
[23] G.L. Hug, B. Marciniak, J. Phys. Chem. 98 (31) (1994) 7523.
[24] B. Marciniak, G.L. Hug, J. Photochem. Photobiol. A: Chem. 78 (1) (1994) 7.
[25] H.D. Mettee, Can. J. Chem. 45 (4) (1967) 339.
[26] A. Gaplovsky, S. Toma, J.L. Luche, T. Kimura, B. Jakubikova, K. Gaplovska, J. Photochem. Photobiol. A: Chem. 152 (2002) 135.
[27] K.H. Park, S.J. Oh, Phys. Rev. B 48 (1993) 14833.
[28] P.D. Rack, T.A. O'Brien, M.C. Zerner, P.H. Kolloway, J. Appl. Phys. 86 (1999) 2377.
[29] Y.A. Teterin, A.Y. Teterin, A.M. Lebedev, I.O. Utkin, J. Electron. Spectrosc. Relat. Phenom. 88-91 (1998) 275.
[30] D. Briggs, second ed., in: D. Briggs, M.P. Seah (Eds.), Practical Surfaces Analysis, vol. 1, Wiley, New York, 1995, p. 444.
[31] C.D. Wagner, L.E. Davis, M.V. Zeller, J.A. Taylor, R.H. Raymond, L.H. Gale, Surf. Interf. Anal. 3 (1981) 211.